

# Invasive advance of an advantageous mutation: Nucleation theory

Lauren O'Malley<sup>a</sup>, James Basham<sup>a</sup>, Joseph A. Yasi<sup>a,1</sup>, G. Korniss<sup>a</sup>,  
Andrew Allstadt<sup>b</sup>, Thomas Caraco<sup>b,\*</sup>

<sup>a</sup>*Department of Physics, Applied Physics, and Astronomy, Rensselaer Polytechnic Institute, 110 8th Street, Troy, NY 12180-3590, USA*

<sup>b</sup>*Department of Biological Sciences, University at Albany, Albany, NY 12222, USA*

Received 1 December 2005

Available online 27 June 2006

## Abstract

For sedentary organisms with localized reproduction, spatially clustered growth drives the invasive advance of a favorable mutation. We model competition between two alleles where recurrent mutation introduces a genotype with a rate of local propagation exceeding the resident's rate. We capture ecologically important properties of the rare invader's stochastic dynamics by assuming discrete individuals and local neighborhood interactions. To understand how individual-level processes may govern population patterns, we invoke the physical theory for nucleation of spatial systems. Nucleation theory discriminates between single-cluster and multi-cluster dynamics. A sufficiently low mutation rate, or a sufficiently small environment, generates single-cluster dynamics, an inherently stochastic process; a favorable mutation advances only if the invader cluster reaches a critical radius. For this mode of invasion, we identify the probability distribution of waiting times until the favored allele advances to competitive dominance, and we ask how the critical cluster size varies as propagation or mortality rates vary. Increasing the mutation rate or system size generates multi-cluster invasion, where spatial averaging produces nearly deterministic global dynamics. For this process, an analytical approximation from nucleation theory, called Avrami's Law, describes the time-dependent behavior of the genotype densities with remarkable accuracy.  
© 2006 Elsevier Inc. All rights reserved.

*Keywords:* Critical radius; Ecological invasion; Individual-based models; Preemptive competition; Recurrent mutation; Spatial clustering

## 1. Introduction

Understanding how localized biotic interactions govern invasion dynamics and an invader's subsequent spatial expansion remains a fundamental challenge in population biology (Levin et al., 1997; Wilson, 1998). Fisher (1937) and Kolmogorov et al. (1937) provided initial insight; they demonstrated how spatially structured dispersal can organize the advance of a favorable mutation. Fisher (1937) approximated the genetic process with a reaction–diffusion equation, and diffusion theory has since served repeatedly to model spatial expansion in ecology, evolution and epidemiology (reviewed by Fife, 1979; Okubo, 1980;

Holmes et al., 1994; Murray, 2003). Generalizations of basic reaction–diffusion theory, intended to enhance biological realism, include models with age-dependent birth and death rates (Frantzen and van den Bosch, 2000; Neubert and Caswell, 2000), non-normal dispersal kernels (Kot et al., 1996; see Chesson and Lee, 2005), spatial heterogeneity (Cantrell and Cosner, 1991), and granularity of space or time (Neubert et al., 1995). Most of these analyses neglect demographic stochasticity, which can be important at local introduction of a rare type, to focus on the velocity of a travelling wave propelling an invader's spatial advance (van den Bosch et al., 1990; Caraco et al., 2002; O'Malley et al., in press; see Lewis and Pacala, 2000). Metz et al. (2000) provide a useful guide to biological generalizations of diffusion processes.

Diffusion models sometimes predict velocities of spatial advance with accuracy, from the scale of nearest-neighbor infection (Zadoks, 2000) to biogeographic range expansion (van den Bosch et al., 1992). But travelling waves permit

\*Corresponding author.

*E-mail addresses:* [omalll@rpi.edu](mailto:omalll@rpi.edu) (L. O'Malley), [bashaj@rpi.edu](mailto:bashaj@rpi.edu) (J. Basham), [yasi@uiuc.edu](mailto:yasi@uiuc.edu) (J.A. Yasi), [korniss@rpi.edu](mailto:korniss@rpi.edu) (G. Korniss), [aa6545@albany.edu](mailto:aa6545@albany.edu) (A. Allstadt), [caraco@albany.edu](mailto:caraco@albany.edu) (T. Caraco).

<sup>1</sup>Present address: Department of Physics, University of Illinois, 1110 West Green Street, Urbana, IL 61801-3080, USA.

infinitely small population densities (van Baalen and Rand, 1998); consequently, the model may fail to capture essential properties of the dynamics of rarity (Durrett and Levin, 1994a), both at introduction and at the edge of an invader's expansion (Ellner et al., 1998; Thomson and Ellner, 2003). An alternative perspective on invasion assumes discrete individuals; individual-based models can directly address the impact of spatially clustered growth on a rare mutation's fate when births and deaths occur as a random process (Claessen and de Roos, 1995; Iwasa et al., 1998; Wei and Krone, 2005; Caraco et al., 2006).

We analyze the spatial dynamics of a two-allele system where discrete individuals compete preemptively. We assume two-way, recurrent mutation in a population propagating clonally; the individual-level assumptions are simple, but the system's behavior can be complex. Mutation, introducing a superior allele, is a rare process, but can potentially occur anywhere in the spatial system. Each introduction initiates a separate cluster of invaders; a cluster may disappear through mortality, or may grow large. Our main results show how patterns in an advantageous mutation's spatial clustering influence the time elapsing until the superior allele replaces the resident. In particular, we present a novel dependence of an inferior allele's "lifetime" on the probabilistic rate of mutation.

To address the system's population-level behavior, we invoke the theory for homogeneous nucleation of spatial systems (Kolmogorov, 1937; Johnson and Mehl, 1939; Avrami, 1940). Nucleation theory offers novel characterizations of the genetic or ecological clustering found in populations with locally structured interactions (Gandhi et al., 1999; Korniss and Caraco, 2005). Expanding upon our preliminary analysis (Yasi et al., in press), we apply nucleation theory to the spread of an advantageous mutation. Foremost, we want to predict the time-dependent, global genotype densities, which are driven by locally clustered growth of the favored allele. To do so, we employ a powerful approximation, called Avrami's Law (Ishibashi and Takagi, 1971; Rikvold et al., 1994; Korniss et al., 1999; Ramos et al., 1999) that describes our simulated mutation-selection dynamics quite accurately. We offer some new predictions about temporal behavior of spatially structured competitive systems, and suggest a framework for developing new ideas concerning spatially explicit invasion dynamics.

In Section 2, we describe the details of our model. Section 3 examines conditions for equilibrium behavior, and the transitions between equilibria. To emphasize the impact of spatial structure, we compare equilibrium phase transitions observed in simulation to the model's mean-field (MF) approximation and its pair approximation (PA). We relegate details of the MF analysis, and some results on approach to population extinction, to Appendix A. We analyze a PA in Appendix B. Section 4 contrasts single-cluster and multi-cluster invasion processes, motivating the application of nucleation theory in Section 5. In Section 6, we use the theory to interpret the simulated dynamics.

Section 7 summarizes our results and discusses further applications of nucleation theory in evolutionary ecology.

## 2. Spatial model

We consider an  $L \times L$  lattice with periodic boundaries; a lattice site represents the minimal level of local resources required to sustain a single organism. Hence each site is either empty or occupied by one haploid individual (a resident or an invader). The local occupation numbers at site  $\mathbf{x}$ ,  $n_g(\mathbf{x}) = 0, 1$ ;  $g = 1, 2$ , count the number of resident and invader genotypes, respectively.

Competition for space is preemptive (Amarasekare, 2003; Shurin et al., 2004; Tainaka et al., 2004); an individual of either genotype may propagate clonally only if one or more of the  $\delta$  nearest neighboring sites is empty. Specifically, if site  $\mathbf{x}$  is empty, that site is colonized by allele  $g$  at total probabilistic rate  $\alpha_g \eta_g(\mathbf{x})$ .  $\alpha_g$  is the per-individual propagation rate of allele  $g$ .  $\eta_g(\mathbf{x})$  is the density of allele  $g$  on  $\sigma(\mathbf{x})$ , the set of nearest neighbors of site  $\mathbf{x}$ . Since the size of the interaction neighborhood is  $|\sigma(\mathbf{x})| = \delta$ , we have

$$\eta_g(\mathbf{x}) = (1/\delta) \sum_{\mathbf{x}' \in \sigma(\mathbf{x})} n_g(\mathbf{x}'). \quad (1)$$

Most of our analyses below take  $\delta = 4$ , the four nearest neighbors on a square lattice. Unless noted explicitly in the figures, results are for  $\delta = 4$ . To test the robustness of some of our findings, we also considered neighborhood sizes  $\delta = 8$  and 12.

When the invader allele has a reproductive advantage,  $\alpha_2 > \alpha_1$ ; we shall assume this condition holds when we analyze invasion with nucleation theory (Sections 4–6). We assume two-way, recurrent mutation. Each individual of genotype  $g$  independently mutates to genotype  $(1 + |g - 2|)$  at constant probabilistic rate  $\phi_g$ . Finally, each individual carrying allele  $g$  suffers mortality at probabilistic rate  $\mu_g$ .

We have a particular interest in the way clonal propagation, through direct effects on cluster-size dynamics, drives competition between populations (O'Malley et al., 2005). Therefore, we let  $\mu_1 = \mu_2 = \mu$ , and  $\phi_1 = \phi_2 = \phi$ . The sole difference between genotypes is the difference in propagation rates. We summarize the local transition rates for an arbitrary site  $\mathbf{x}$  as

$$0 \xrightarrow{\alpha_1 \eta_1(\mathbf{x})} 1, \quad 0 \xrightarrow{\alpha_2 \eta_2(\mathbf{x})} 2, \quad 1 \xrightarrow{\mu} 0, \quad 2 \xrightarrow{\mu} 0, \quad 1 \overset{\phi}{\leftrightarrow} 2, \quad (2)$$

where 0,1,2 indicates whether the site is empty, occupied by the resident genotype, or occupied by the invader genotype, respectively. We list the paper's symbols in Table 1.

## 3. Equilibrium phase diagram

Although this paper focuses on the dynamics of an advantageous allele's invasion, it is instructive to begin with a general picture of the model's underlying equilibrium phases. Our assumptions imply strong spatial clustering of the invasion process. Therefore, both MF

Table 1  
Definitions of model symbols (numerical value or range used in simulations, where appropriate)

Symbol	Definition
$L$	Lattice length/width ( $16 \leq L \leq 1000$ )
$n_1(\mathbf{x})$	Local occupation numbers for the resident allele at site $\mathbf{x}$ ( $n_1(\mathbf{x}) = 0,1$ )
$n_2(\mathbf{x})$	Local occupation numbers for the invasive allele at site $\mathbf{x}$ ( $n_2(\mathbf{x}) = 0,1$ )
$\sigma(\mathbf{x})$	Set of nearest neighbors of site $\mathbf{x}$
$\delta$	Neighborhood size for local propagation ( $\delta =  \sigma(\mathbf{x}) $ )
$\eta_g(\mathbf{x})$	Density of allele $g$ on $\sigma(\mathbf{x})$ ( $g = 1, 2$ )
$\phi$	Recurrent (forward–backward) mutation rate ( $10^{-8} \leq \phi \leq 10^{-2}$ )
$\alpha_1$	Resident allele's clonal propagation rate
$\alpha_2$	Invasive allele's clonal propagation rate
$\mu_1$	Resident allele's mortality rate
$\mu_2$	Invasive allele's mortality rate ( $\mu_1 = \mu_2 = \mu$ )
$\rho_1(t)$	Resident allele's global density
$\rho_2(t)$	Invasive allele's global density
$\rho_1^*$	Resident's "metastable" global density
$\rho_2^*$	Invader's global density at equilibrium
$\beta$	Critical exponent for the global density near the continuous equilibrium phase transition associated with dispersal-limited extinction
$\langle \tau \rangle$	Resident's metastable lifetime
$\langle t_n \rangle$	Average waiting time for invader's nucleation
$t_g$	Time for successful invader to grow to competitive dominance
$I$	Nucleation rate per unit area
$v$	Velocity at which cluster radius grows
$R_c$	Critical radius of nucleating cluster
$R_d$	Average separation of nucleating invasive clusters

approximation, which assumes homogeneous mixing, and ordinary PA, which tracks correlations of nearest neighbors, will fail to capture relevant characteristics of the spatiotemporal invasion dynamics. Nevertheless, each yields a *qualitatively* correct equilibrium phase diagram; we present details in Appendix A. Here, we establish a context for applying nucleation theory by sketching the equilibrium phase diagram, obtained through Monte Carlo (MC) simulation, for the fully detailed spatial model.

Using the local transition rates given by Expression (2), we carried out MC simulations on  $L \times L$  square lattices with periodic boundary conditions. The system exhibits three equilibrium phases [Fig. 1(a)]: mutual extinction ("phase 0") for  $\alpha_1 < \alpha_c$  and  $\alpha_2 < \alpha_c$  (where  $\alpha_c$  depends on  $\mu$  approximately as  $\alpha_c \approx 1.65\mu$ ); competitive dominance by allele 1 ("phase 1") for  $\alpha_1 > \alpha_c$  and  $\alpha_1 > \alpha_2$ ; and, by symmetry, competitive dominance by allele 2 ("phase 2") for  $\alpha_2 > \alpha_c$  and  $\alpha_1 < \alpha_2$ . In the latter two phases, the competitively inferior allele appears only through unstable local fluctuations due to rare mutations, which generate a very small global density (of order  $\phi$ ). The main features of the equilibrium transitions between the above phases are shown in Figs. 1(b) and (c), and are discussed in detail in Appendix A. Our later analyses emphasize the *dynamical* transformation between phases 1 and 2. In particular, we consider the system initially in phase 1 (allele 1, the resident, at equilibrium), with a competitively superior allele appearing through rare mutations (introducing allele 2, the invader). Next, we characterize the spatiotemporal behavior of this invasion process, which leads, of course, to competitive dominance by allele 2.

#### 4. Critical cluster size, single-cluster and multi-cluster invasion

Away from dispersal-limited extinction (see Appendix A), each allele can persist dynamically in the other's absence, but allele 2, the invader, has a clonal-propagation advantage. We assume that mutation is rare, and restrict attention to the parameter regime where  $\phi \ll \alpha_c < \alpha_1 < \alpha_2$  and  $\phi \ll (\alpha_2 - \alpha_1)$ , i.e., the region where the invader will eventually exclude the resident.

We performed extensive simulations of our model's invasion dynamics. The time unit was one Monte Carlo step per site (MCSS) during which  $L^2$  lattice sites were chosen randomly and updated probabilistically. These procedures mimic continuous-time stochastic dynamics in the large  $L$  limit (Durrett and Levin, 1994b; Korniss et al., 1999). We initialized each simulation with every site occupied by allele 1. Allele 2 entered through rare, recurrent mutation.

Nucleation theory predicts that the invader allele will statistically tend to advance only if it generates a cluster sufficiently large that the probability it will grow at its periphery exceeds  $\frac{1}{2}$ . For realistic spatial scales, there should exist a critical radius for invader clusters; smaller clusters tend to decrease in size, and larger clusters tend to grow (Gandhi et al., 1999; Korniss et al., 1999; O'Malley et al., 2005). Snapshots of simulation configurations reveal strongly clustered invader growth, and confirm the existence of a critical radius  $R_c$ , hence a critical cluster size, which we analyze below.

For given parameter values, there also exists a characteristic length scale  $R_d$ , the typical distance separating

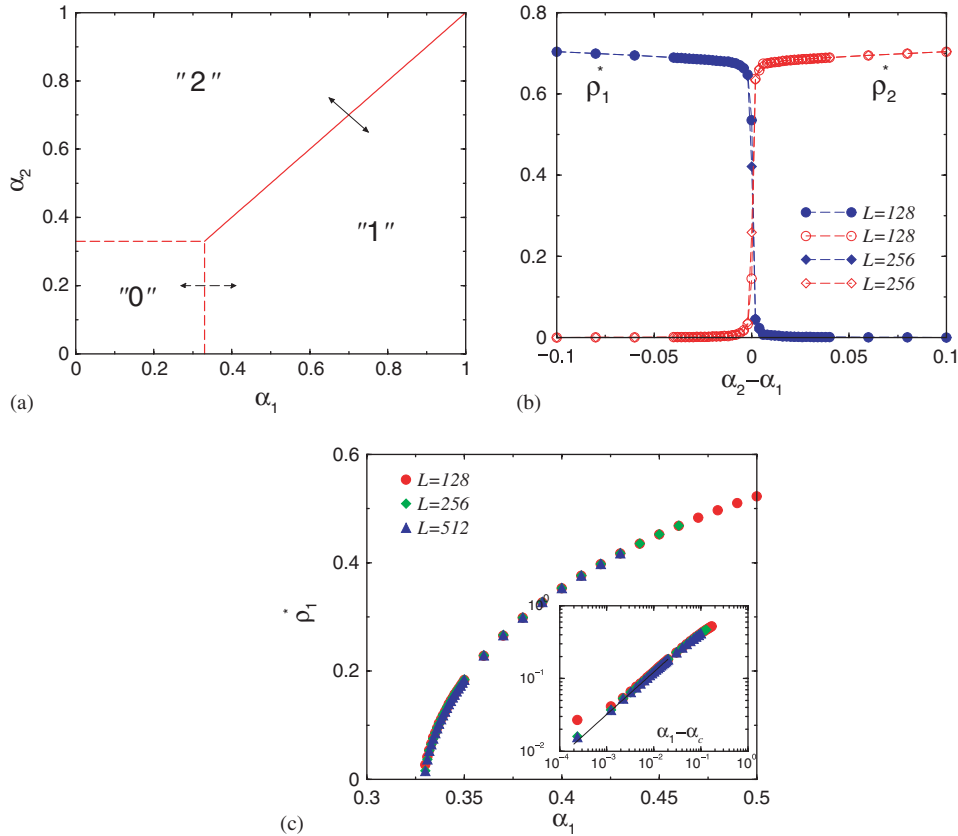


Fig. 1. (a) Equilibrium phase diagram of the two-allele system (obtained by Monte Carlo simulations) in the  $\alpha_1$ - $\alpha_2$  plane for  $\mu = 0.20$  and  $\phi = 10^{-5}$ . Arrows indicate where the phase boundaries were crossed, detailed in figures (b) and (c). (b) Sharp crossover between the two active (i.e., competitively dominant) phases, viewed perpendicularly to the  $\alpha_1 = \alpha_2$  symmetry axis at  $\alpha_1 = \alpha_2 = 0.70$ , controlled by the difference  $\alpha_2 - \alpha_1$ . (c) Continuous phase transition between the active (phase 1) and the absorbing (phase 0) phases. MC simulation data is shown for various system sizes for fixed  $\alpha_2 = 0.20$  with  $\alpha_1$  varied. The inset indicates the power-law behavior of the density of allele 1, consistent with the DP universality class; see Appendix A.

invading clusters. For  $L \ll R_d$ , invasion almost always occurs through the spread of a single invading cluster (single-cluster invasion), while for  $L \gg R_d$ , the invasion results from many invading clusters (multi-cluster invasion). Conversely, when we fix linear system size  $L$  and all other parameters except the mutation rate  $\phi$ , the characteristic length scale  $R_d$  becomes a function of  $\phi$ . For this case, there is a characteristic value of  $\phi$  such that for a sufficiently rare occurrence of mutation, multi-cluster invasion by the favored allele crosses over to the single-cluster geometry. These two different invasion modes, single-cluster and multi-cluster, are illustrated by configuration snapshots in Figs. 2 and 3, respectively. Importantly, these different modes of spatial growth are associated with drastically different sets of dynamical properties, as can be seen from the time series of the global densities in Fig. 4. In the single-cluster regime, the waiting time until the first (and almost always the only) successful invader cluster appears is inherently stochastic [Fig. 4(a)]; the standard deviation of the time elapsing until the invader outnumbers the resident (the system lifetime) is comparable to its mean. In contrast, in the multi-cluster regime, global densities exhibit a near-deterministic lifetime [Fig. 4(b)].

For either invasion mode, we consider the invader allele competitively dominant when the resident allele's global density first falls to one-half its quasi-equilibrium density (in the absence of the invader)  $\rho_1^*$ . That is, the invader dominates when  $\rho_1(t)|_{t=\tau} = \rho_1^*/2$ . Hence, given that we gauge the invader allele's advance by quantifying the resident's decay, we define the non-negative random variable  $\tau$  as the first-passage time of the resident's density to  $\rho_1^*/2$ . We refer to the expected value  $\langle \tau \rangle$  as the resident allele's "metastable" lifetime (Rikvold et al., 1994; Korniss and Caraco, 2005).

### 5. Homogeneous nucleation and growth

The preceding observations justify applying the theory of homogeneous nucleation and growth (Kolmogorov, 1937; Johnson and Mehl, 1939; Avrami, 1940) to predict important characteristics of the advantageous allele's spread. This framework, often referred to as KJMA theory or Avrami's Law, has successfully described conceptually analogous dynamic phenomena in physics (Ishibashi and Takagi, 1971; Duiker and Beale, 1990; Rikvold et al., 1994; Richards et al., 1995; Ramos et al., 1999; Korniss et al., 1999), chemistry (Ben-Naim and Krapivsky, 1996;

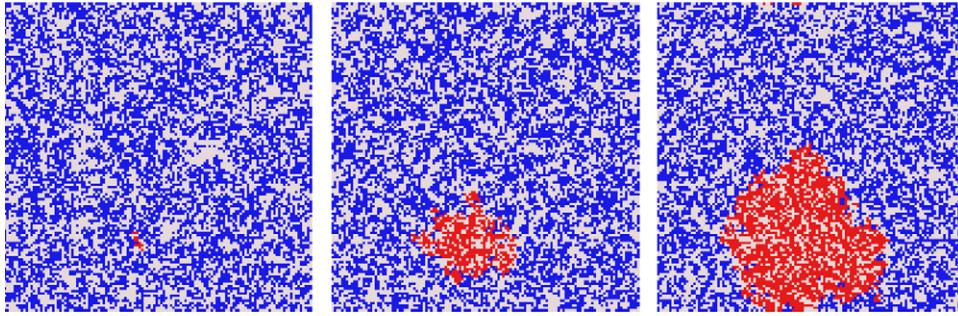


Fig. 2. Single-cluster invasive spread. Configuration snapshots from Monte Carlo simulations for  $L = 128$ ,  $\alpha_1 = 0.50$ ,  $\alpha_2 = 0.70$ ,  $\mu = 0.20$ , and  $\phi = 10^{-7}$ . White represents empty sites, blue and red correspond to sites occupied by the resident and the invasive allele, respectively. Configurations are shown (from left to right) at  $t = 2100$ ,  $2300$ , and  $2500$  (in units of MCSS).

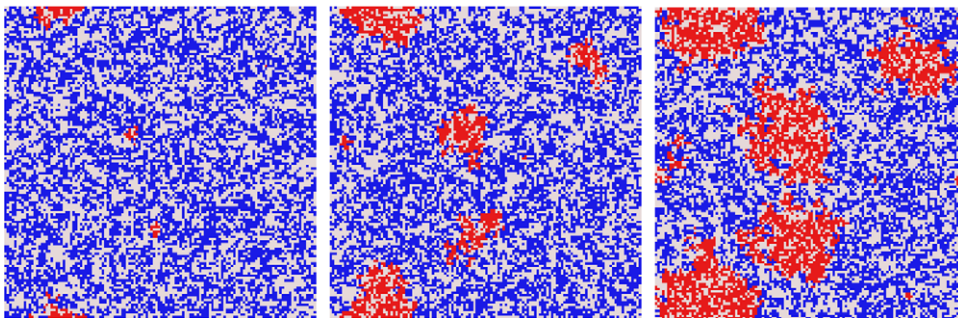


Fig. 3. Multi-cluster invasive spread. Configuration snapshots from Monte Carlo simulations for  $L = 128$ ,  $\alpha_1 = 0.50$ ,  $\alpha_2 = 0.70$ ,  $\mu = 0.20$ , and  $\phi = 10^{-5}$ . White represents empty sites, blue and red correspond to sites occupied by the resident and the invasive allele, respectively. Configurations are shown (from left to right) at  $t = 100$ ,  $200$ , and  $300$  (in units of MCSS).

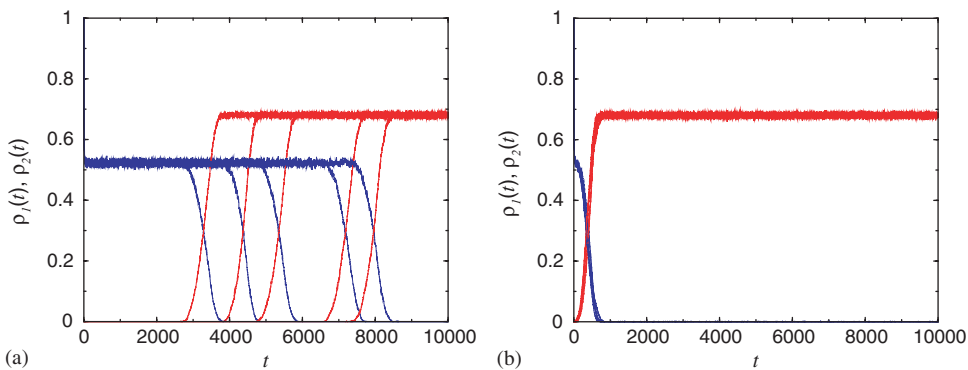


Fig. 4. Time-dependent global densities (five independent realizations) of the two alleles in (a) single-cluster and (b) multi-cluster invasion. Matching pairs of  $\rho_1(t)$  and  $\rho_2(t)$  intersect near a density of 0.3. Parameters are the same as those in Figs. 2 and 3 for (a) and (b), respectively.

Karttunen et al., 1998; Machado et al., 2005), DNA replication (Herrick et al., 2002), and certain spatially structured ecological interactions (Korniss and Caraco, 2005; O'Malley et al., 2005).

A simple application of KJMA theory to our model assumes that nucleation of a successful invading cluster is a Poisson process with a constant (in both space and time) nucleation rate per unit area  $I$ . Further, the theory assumes that once a successful cluster of the advantageous allele has been nucleated, it grows deterministically with a constant radial velocity  $v$ . Here, we briefly present the main features of Avrami's Law and then summarize a scaling argument

(Rikvold et al., 1994; Ramos et al., 1999) that identifies the time and length scales governing single-cluster versus multi-cluster invasion.

For small spatial systems, where  $L \ll R_d$  ( $R_d$  to be determined), the invasive allele advances as a single invading cluster, the first cluster that nucleates and sweeps through the environment before another appears (Rikvold et al., 1994; Richards et al., 1995; Korniss and Caraco, 2005). Since nucleation of a successful invasive cluster is a Poisson process, the cumulative probability distribution of waiting times for single-cluster invasion should have a characteristic form. That is,  $P_{\text{not}}(t) = \Pr[\tau > t]$ , the

probability that the resident's global density has not decayed to  $\rho_1^*/2$  by time  $t$ , when the first and only invading cluster drives the resident's decline, will be exponential:

$$P_{\text{not}}(t) = \begin{cases} 1 & \text{for } t \leq t_g, \\ \exp[-(t - t_g)/\langle t_n \rangle] & \text{for } t > t_g. \end{cases} \quad (3)$$

Here,  $\langle t_n \rangle = (L^2 I)^{-1}$  is the average time elapsing until nucleation occurs, and  $t_g \sim L/v$  is the approximately deterministic growth time until the invading allele drives the resident to half its initial density. For very small nucleation rates per unit area, we have  $\langle t_n \rangle \gg t_g$ . Therefore, the lifetime of the resident allele is governed by the large average waiting times until the first successful cluster of the invasive allele nucleates, so that  $\langle \tau \rangle = \langle t_n \rangle + t_g \approx \langle t_n \rangle$ .

For large spatial systems,  $L \gg R_d$ , so that system size exceeds the typical distance between invader clusters. Therefore, many randomly nucleated and expanding clusters of the favored allele contribute to the resident allele's decline. In the limit of  $L \rightarrow \infty$ , the global dynamics approaches deterministic functions. The number of invader clusters grows large, so that spatial averaging of their behavior strongly limits stochastic fluctuations at the global level. As a direct consequence,  $P_{\text{not}}(t)$  approaches a step-function centered on the system-size independent lifetime  $\langle \tau \rangle$ . In this large-system limit,  $R_c \ll R_d \ll L$ , and the global densities can be approximated closely by Avrami's Law applied to a two-dimensional system (Kolmogorov, 1937; Johnson and Mehl, 1939; Avrami, 1940). The original studies develop Avrami's Law in detail, and a number of more recent papers (e.g., Ishibashi and Takagi, 1971; Korniss and Caraco, 2005) sketch derivations of the main result. Essentially, Avrami's Law approximates the aggregate consequence of invading clusters that nucleate randomly and independently in space and time. Given that nucleation occurs at constant rate per unit area  $I$ , and that each cluster subsequently grows at constant radial velocity  $v$ , we have the global densities:

$$\begin{aligned} \rho_1(t) &\approx \rho_1^* \exp \left[ -\ln(2) \left( \frac{t}{\langle \tau \rangle} \right)^3 \right], \\ \rho_2(t) &\approx \rho_2^* \left( 1 - \exp \left[ -\ln(2) \left( \frac{t}{\langle \tau \rangle} \right)^3 \right] \right), \end{aligned} \quad (4)$$

where the characteristic time (the lifetime)  $\langle \tau \rangle$  depends on  $I$  and  $v$ .

This dependence suggests a context for linking global dynamics and individual-level interactions. While a detailed derivation of Avrami's Law provides the dependence of the residents' lifetime  $\tau \equiv \langle \tau \rangle$  on  $I$  and  $v$ , one can extract these dependencies by basic scaling considerations (Rikvold et al., 1994; Ramos et al., 1999). The average diameter of invader clusters at time  $t = \tau$  scales as  $v\tau$ , assuming a constant radial-growth velocity. Considering the size to which a cluster can grow without contacting another, the average spatial separation between the centers of invader

clusters should scale similarly at time  $t = \tau$ , thus  $R_d \sim v\tau$ . Further, at the same instant, on average, one cluster has nucleated in a corresponding area of diameter  $R_d$ ; thus, in two dimensions,  $I R_d^2 \tau \sim 1$ . Hence, one obtains:

$$\tau \sim (I v^2)^{-1/3}, \quad (5)$$

and

$$R_d \sim \left( \frac{v}{I} \right)^{1/3}. \quad (6)$$

Expression (5) gives the characteristic time scale, and Expression (6) gives the characteristic length scale of the system in the limit of  $L \rightarrow \infty$ . We infer the following from Expression (5). The parameters of a specific model for spatially structured ecological interactions (i.e., local transition rates  $\phi, \alpha_1, \alpha_2, \mu$ , and  $\delta$ ) govern the characteristic time scale (the lifetime  $\tau$ ) through their impact on  $I$ , the superior allele's nucleation rate per unit area, and on  $v$ , the radial growth velocity of the invading clusters. Expression (5) suggests that the time elapsing until the invader dominates the resident will vary with the inverse of the cube root of the rate at which invader clusters reach critical size (i.e., nucleate); for discussion, see Korniss and Caraco (2005).

## 6. Simulation results and interpretation

To further our understanding of nucleation, we conducted separate simulations to ask how model parameters affect critical cluster size, hence the critical radius  $R_c$ . Recall that at critical size, growth and decay of a cluster have equal probability. For this analysis only, we began each simulation by placing a single favored-allele cluster, of a selected size [and with a "round" shape,  $A(0) \sim R^2(0)$ ], on the lattice. We set the mutation rate  $\phi = 0$ , so the invader cluster's dynamics depended on propagation and mortality only. If the invader declined to extinction, we recorded the elapsed time. Otherwise, the invader advanced to competitive dominance, and we recorded the time at which the resident's global density first decayed to  $\rho_1^*/2$  (invasion time).

Geometric considerations suggest that  $R_c$  will increase as the difference between propagation rates ( $\alpha_2 - \alpha_1$ ) declines. Consider an empty site in the vicinity of the front separating the invader cluster and the resident. For sufficiently small invader clusters, the correspondingly large curvature implies that the invader will occupy only a small fraction of the neighborhood around the open site (Gandhi et al., 1999). Hence, the resident will have an advantage in colonizing the open site, due simply to its superior numbers (and not due to ecological superiority). However, for larger invader clusters the curvature becomes sufficiently shallow that the invader's greater propagation rate will prevail over the more numerous residents. As the difference between the individual-level propagation rates decreases, a larger (critical) radius is needed for the invader to overcome the locally more numerous resident, and

prevail. An increased mortality rate should open more sites for neighborhood growth of the superior allele, somewhat relaxing the constraints of preemptive competition (Korniss and Caraco, 2005).

For each initial cluster size and  $(\alpha_g, \mu)$ -combination, we plotted the fraction of  $10^4$  simulations where the favored allele invaded the resident; by definition, this fraction (the relative success rate) is  $\frac{1}{2}$  at the critical cluster size. For mortality rates  $\mu = 0.1$  and  $0.2$ , Fig. 5(a) shows how the relative success rate changes as the resident's propagation rate  $\alpha_1$  increases toward the invader's propagation rate  $\alpha_2$ , and implies, in turn, how the critical cluster size increases at the same time. Fig. 5(a) also indicates that doubling the mortality rate ( $\mu = 0.1$ – $0.2$ ) had little influence on critical cluster size for the given  $\alpha_g$ . However, greater mortality reduced the resident allele's metastable lifetime. Fig. 5(b) shows that when the favored allele advanced, greater mortality nearly halved the mean time for the resident's decay; the global dynamics was accelerated.

### 6.1. Single-cluster invasion

To analyze single-cluster invasion, we fixed  $\alpha_1 = 0.5$ , and  $\alpha_2 = 0.7$ , for system sizes  $L = 16, 32$ , and  $64$ . For three values of the mortality rate,  $\mu = 0.1, 0.15$ , and  $0.2$ , we consider mutation rates  $10^{-7} \leq \phi \leq 10^{-5}$ . Single-cluster invasion is inherently stochastic, and must be analyzed probabilistically. While local mutation occurs as a Poisson process, it is not known a priori if the nucleation of a "supercritical" cluster will also be Poisson. Therefore, for simulations in the single-cluster regime, we constructed cumulative probability distributions for the lifetime of the resident allele  $P_{\text{noit}}(t)$ , i.e., the probability that the resident's global density has not yet declined below  $\rho_1^*/2$  by time  $t$ .

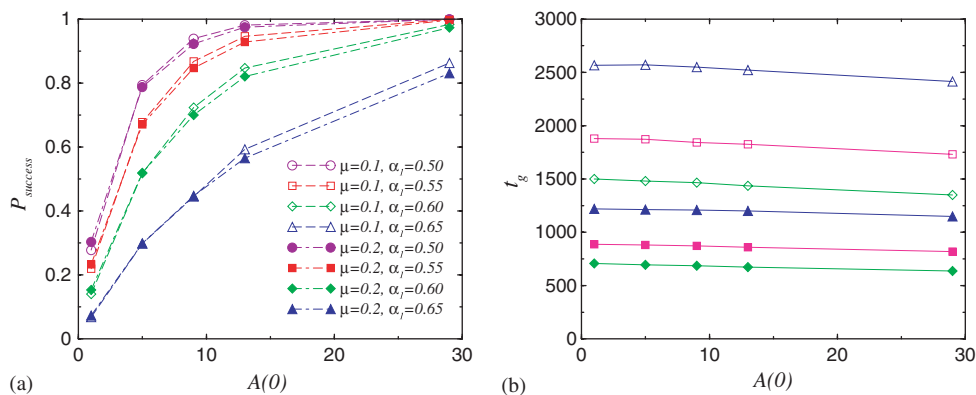


Fig. 5. (a) Fraction of successful invasions vs. initial size of the cluster of the favored allele for two different values of the mortality rate [ $\mu = 0.1$  (open symbols),  $0.2$  (solid symbols)] and four different values of the propagation rate of the resident allele ( $\alpha_1 = 0.5, 0.55, 0.60, 0.65$ ) when invader propagation rate  $\alpha_2 = 0.7$ ,  $L = 64$ . Abscissa shows size (number of sites) of single invasive-allele cluster at initiation of simulation. Ordinate is the fraction of  $10^4$  simulations resulting in successful advance of favored allele when further mutation has been eliminated. At critical cluster size invasion fraction is  $0.5$ , by definition. Critical cluster size increases as difference between invader and resident propagation rates declines. Increasing the common mortality rate ( $0.1$ – $0.2$ ) has little effect on critical cluster size for given  $\alpha_g$  values. (b) Invasion times for successful invasions. Abscissa shows size of single invasive-allele cluster at initiation of simulation. Ordinate is time (MCSS) at which resident allele's global density first falls to half its equilibrium density in absence of favored allele.  $\alpha_2 = 0.7$ ,  $L = 64$ .  $(\alpha_1, \mu)$  combinations are  $(0.6, 0.1)$  [open diamonds],  $(0.625, 0.1)$  [open squares],  $(0.65, 0.1)$ , [open triangles];  $(0.6, 0.2)$  [solid diamonds],  $(0.625, 0.2)$  [solid squares], and  $(0.65, 0.2)$ , [solid triangles]. Given the  $\alpha_g$  values, increased mortality accelerates invasion dynamics and decreases time at which favored allele attains competitive superiority.

We found that the distributions are indeed exponentials, in accordance with Eq. (3). Fig. 6(a) shows results for three mutation rates, given a fixed (sufficiently small) system size and fixed mortality rate. We obtained the average nucleation times  $\langle t_n \rangle$  from the slopes of the exponential distributions; see Fig. 6(b). These results, in turn, yield the mutation-rate dependence of the nucleation rate per unit area  $I(\phi)$ . From Fig. 6(b) we deduce that, for fixed linear system size  $L$ ,  $\langle t_n \rangle \sim \phi^{-1}$ . Therefore, because  $\langle t_n \rangle = (IL^2)^{-1}$ ,  $I(\phi) \sim \langle t_n \rangle^{-1} \sim \phi$ ; the rate at which a critical cluster forms scales with the mutation rate. We also analyzed the system-size dependence (within the single-cluster regime) of the average nucleation time, again, by determining the slopes of the cumulative lifetime distributions for various system sizes [Fig. 7(a)]. We found that the mean waiting time for nucleation of a critical cluster  $\langle t_n \rangle \sim L^{-2}$ ; see Fig. 7(b).

In the single-cluster regime, the advance of the invasive allele (and decline of the resident) exhibits significant stochastic variation; as noted above, the standard deviation of the resident's lifetime  $\tau$  is as large as its mean. The spread of the advantageous mutation is initiated and completed by the first randomly nucleated, successful cluster of the favored allele. Any number of smaller clusters may fail to grow before the successful nucleation event occurs. For very low values of the mutation rate  $\phi$ , the lifetime is dominated by the very large expected waiting time for nucleation, hence:

$$\langle \tau \rangle = \langle t_n \rangle + t_g \approx \langle t_n \rangle \sim \phi^{-1}. \tag{7}$$

### 6.2. Multi-cluster invasion

In the multi-cluster regime the dynamics of the advantageous allele's global density behaves more predictably.

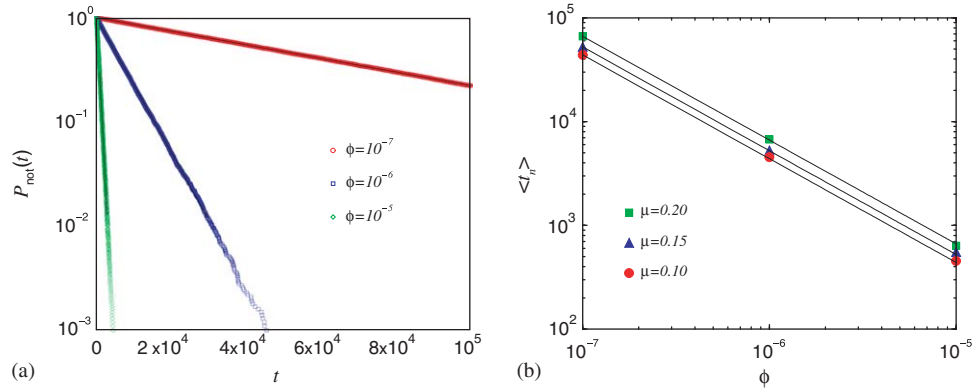


Fig. 6. (a) Cumulative lifetime distributions in single-cluster invasion for  $L = 32$ ,  $\alpha_1 = 0.50$ ,  $\alpha_2 = 0.70$ , and  $\mu = 0.20$ , for three different values of  $\phi$ . (b) Average nucleation times (obtained as the inverse slopes of the exponential distributions) as a function of the mutation rate  $\phi$  for three different values of  $\mu$ . The straight solid lines correspond to  $\langle t_n \rangle \sim \phi^{-1}$ .

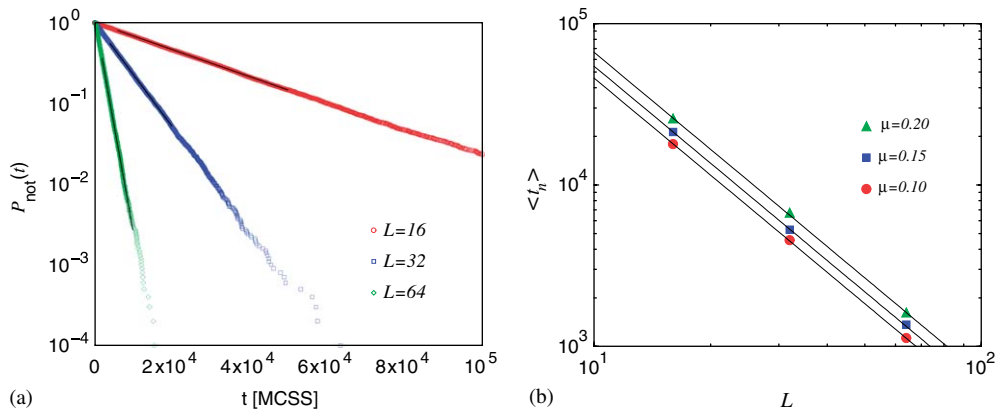


Fig. 7. (a) Cumulative lifetime distributions in single-cluster invasion for  $\phi = 10^{-6}$ ,  $\alpha_1 = 0.50$ ,  $\alpha_2 = 0.70$ , and  $\mu = 0.20$ , for three different values of  $L$ . (b) Average nucleation times (obtained as the inverse slopes of the exponentials) as a function of the linear system size  $L$ . The straight solid lines correspond to  $\langle t_n \rangle \sim L^{-2}$ .

Nucleation and growth of multiple clusters render global densities sums of random variables; spatial averaging within the multi-cluster process reduces variability of the time-dependent global densities among realizations of the dynamics (Rikvold et al., 1994; Ramos et al., 1999; see Wilson et al., 1993). This “self-averaging” induces the nearly deterministic behavior of the global densities in the limit of  $L \rightarrow \infty$ . Therefore, we compared time-dependent global densities observed in our simulations to Avrami’s Law, Eq. (4). Results in Fig. 8 show that it is, indeed, an excellent approximation for times  $t \leq \langle \tau \rangle$ . At times significantly larger than  $\langle \tau \rangle$  invading clusters begin to coalesce, and percolation effects become important.

Assuming that invading clusters spread at a constant velocity, KJMA theory, Expression (5), predicts that the resident allele’s metastable lifetime scales according to

$$\langle \tau \rangle \sim [I(\phi)]^{-1/3} \sim \phi^{-1/3} \quad (8)$$

in the multi-cluster regime. Note the important difference between proportionalities for single and multi-cluster invasion; cf. Eq. (7). The exponent estimated from our simulations, approximately  $-0.3$ , is close to the predicted

value; see Fig. 9. Hence Avrami’s Law described the time course of the resident’s metastable decay with reasonable accuracy. The deviation from prediction likely indicates that, contrary to our assumption, cluster radii, at least for early times, do not grow linearly before reaching a constant radial spreading velocity, which may also be affected by nontrivial properties of the cluster perimeter (cf. Lewis and Kareiva, 1993).

To study robustness of the KJMA-type nucleation and spread of the mutant allele, we also considered neighborhood sizes beyond nearest neighbors ( $\delta = 8$  and  $12$ ). These results are also shown in Figs. 8 and 9(a). Observed global densities are qualitatively similar to those for nearest-neighbor propagation ( $\delta = 4$ ). The shape of the time-dependent global densities is still well approximated by Avrami’s Law, Eq. (4), up to times comparable to  $\langle \tau \rangle$  (Fig. 8), when effects of cluster coalescence become important, and nucleation theory breaks down. Interestingly, the lifetime  $\langle \tau \rangle$  exhibits the same scaling with the mutation rate  $\langle \tau \rangle \sim \phi^{-0.3}$ ; see Fig. 9(a). These results indicate that neighborhood size, hence the opportunity for local dispersal, affects the lifetime through the nucleation rate

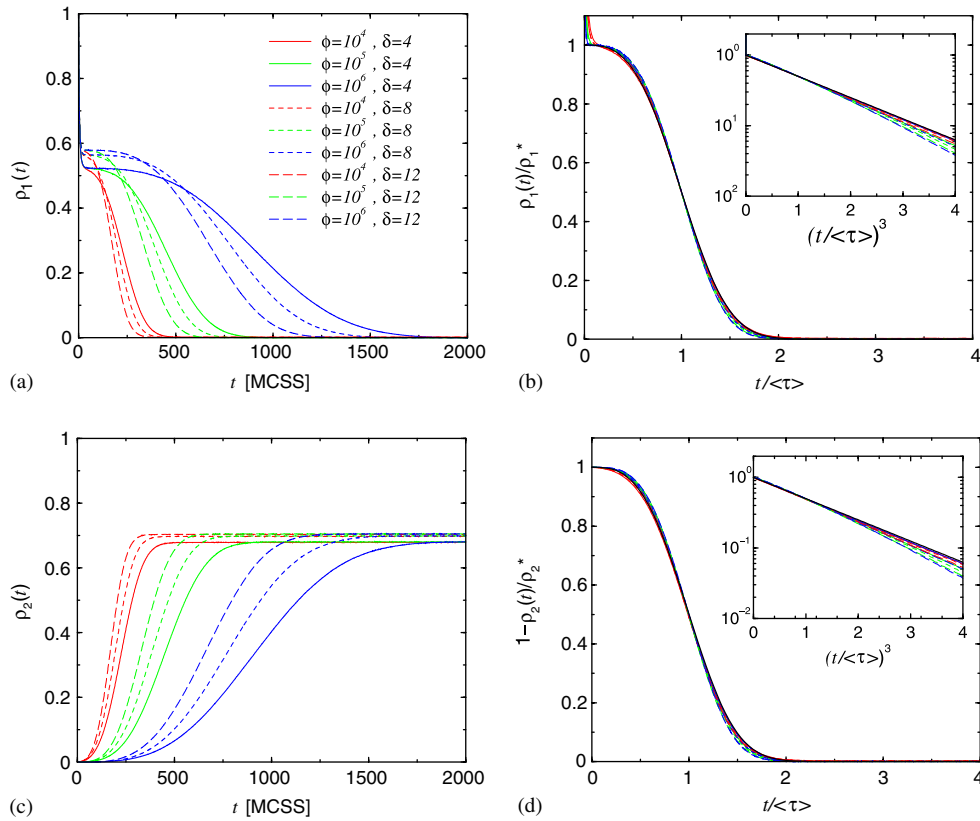


Fig. 8. Time-dependent global densities in the multi-cluster regime for  $L = 1000$ ,  $\alpha_1 = 0.50$ ,  $\alpha_2 = 0.70$ , and  $\mu = 0.20$ , for various neighborhood sizes  $\delta$  and mutation rates  $\phi$ . (a) Time-dependent global density of the resident allele. (b) Scaled time-dependent global density of the resident allele. The bold solid curve corresponds to Avrami's Law, Eq. (4) (hardly distinguishable from the simulation data). The inset shows the same data points, plotting the scaled density vs.  $(t/\langle\tau\rangle)^3$ , on log-linear scales. (c) Time-dependent global density of the invasive allele [symbols same as in (a)]. (d) Scaled time-dependent global density of the invasive allele. The bold solid curve corresponds to Avrami's Law Eq. (4). The inset shows the same data points, plotting the scaled density vs.  $(t/\langle\tau\rangle)^3$ , on log-linear scales.

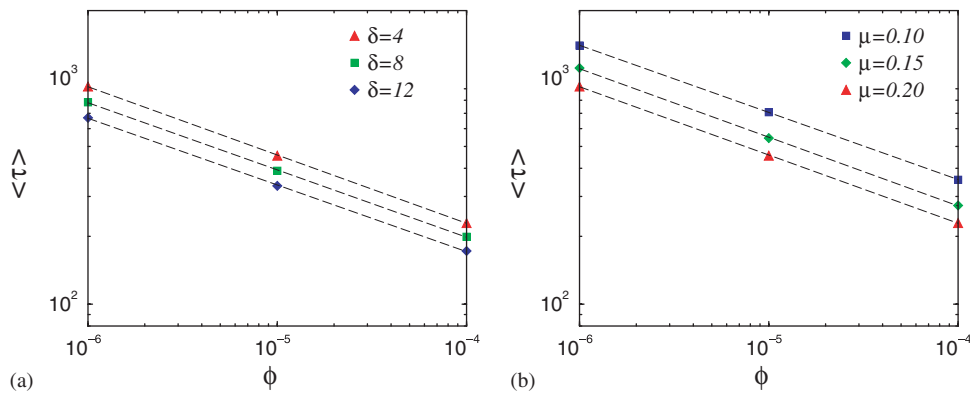


Fig. 9. Average lifetime in the multi-cluster regime (in units of MCSS) vs. the mutation rate  $\phi$  on log–log scales for  $L = 1000$ ,  $\alpha_1 = 0.50$ ,  $\alpha_2 = 0.70$ : (a)  $\mu = 0.20$ , for various neighborhood sizes  $\delta$ ; (b)  $\delta = 4$ , for various values of  $\mu$ . The dashed lines are the fitted slopes, all approximately indicating  $\langle\tau\rangle \sim \phi^{-0.3}$  [cf. Eq. (8)].

per unit area  $I$ , and through  $v$ , the radial growth velocity of each nucleated invader cluster.

### 7. Discussion

We have suggested a new framework for analyzing invasion and spread of a recurring favorable mutation

when competition between genotypes follows locally structured, probabilistic rules. Our study differs from several earlier analyses of spatial competition in that our application of nucleation theory stresses the system's time-dependent characteristics, rather than the asymptotic behavior only. We focused on generic features of the resident allele's lifetime and the global densities, both at a

phenomenological level. Specifically, we emphasized the form of the probability distribution of the resident allele's decay to competitive exclusion in the single-cluster regime, and then emphasized the functional time-dependence of the global allelic densities in the multi-cluster regime. We found that nucleation theory, Avrami's Law in particular, describes the simulated dynamics very well. We detailed quantitative effects of varying both the size of the environment and the rate of mutation. Finally, we indicated that local, measurable rates of propagation and mortality, along with neighborhood size, can affect the scaling of Avrami's Law, hence can affect the global dynamics. Further study will address how variation in local interactions affects nucleation rates pre unit area, cluster growth, and the critical radius.

Fig. 10 summarizes our essential results. For infinitely large systems and sufficiently small mutation rates, the system exhibits multi-cluster invasive spread and is well approximated by Avrami's Law. The self-averaging lifetime of the resident allele scales as  $\langle \tau \rangle \sim \phi^{-0.3}$  (with other parameters fixed). For larger mutation rates, small invasive clusters almost immediately coalesce, and nucleation theory no longer applies. In this regime, MF approximation begins to work reasonably well, since the more numerous small clusters mix almost immediately. For finite systems, however, there is a sufficiently small mutation rate  $\phi$ , such that the typical separation between invasive clusters would become larger than the linear system size ( $R_d \gg L$ ). Here, the invasion dynamics crosses over to the single-cluster mode. For example, if  $L = 64$ , crossover to the single-cluster regime occurs when  $\phi \sim 10^{-5}$ ,

while for  $L = 128$  we noted crossover when  $\phi \sim 10^{-6}$  (Fig. 10). In this regime, the average lifetime (and its standard deviation) scales as  $\langle \tau \rangle \sim \phi^{-1}$ .

The primary feature of our model is that rare random mutations occur independently in space and time, and then initiate invasive clusters. Only some reach a critical size, and continue to grow at their periphery. Once the radius of an invading cluster reaches sufficient length, one can anticipate that the radial velocity approaches its asymptotic value; see Lewis and Kareiva (1993) for deterministic analysis of diffusive ecological invasion in two dimensions (where an "Allee effect" produces another sort of critical radius). Further study of the stochastic interface separating the region of allele 2 from the region of allele 1, and an invader cluster's approach to its asymptotic spreading velocity (O'Malley et al., in press) may provide finer corrections to Avrami's Law for our two-allele model.

We have demonstrated the utility of nucleation theory in a model where the inferior local competitor lacks a compensatory advantage of lower mortality (Caraco et al., 2006) or a larger dispersal profile (Durrett and Levin, 1998; Bolker and Pacala, 1999). Nucleation theory suggests a context for an increased understanding of more complex spatial ecologies. Ideally, an analysis of spatial invasion would reconcile results of individual-based simulations with predictions deduced from tractable mathematical models. For example, Wilson (1998) resolves differences between simulation of a spatially structured predator-prey interaction and an elaboration of a corresponding diffusion model. As indicated above, we anticipate that detailed analysis of the critical radius will yield ecologically detailed hypotheses linking local interaction and population processes. Finally, the framework for analyzing invasive growth suggested here may be extended to more general problems involving temporal variation or spatial heterogeneity in demographic rates (Chesson, 2000; Korniss and Caraco, 2005; Seabloom et al., 2005).

### Acknowledgments

We gratefully acknowledge discussions with Z. Rácz, P.A. Rikvold, M.A. Novotny, T. Ala-Nissila, Z. Toroczka, I.-N. Wang and G. Robinson. We also thank Z. Toroczka for providing us with the code for the numerical integration of the mean-field and pair-approximation dynamics. This material is based upon work supported by the National Science Foundation under Grant No. DEB-0342689. G.K. was also supported in part by NSF through Grant DMR-0426488 and by the Research Corporation through Grant No. RI0761.

### Appendix A. Equilibrium phase diagram and transitions

#### A.1. Mean-field approximation

The mean-field (MF) approximation assumes homogeneous mixing, and so offers a useful comparison to the

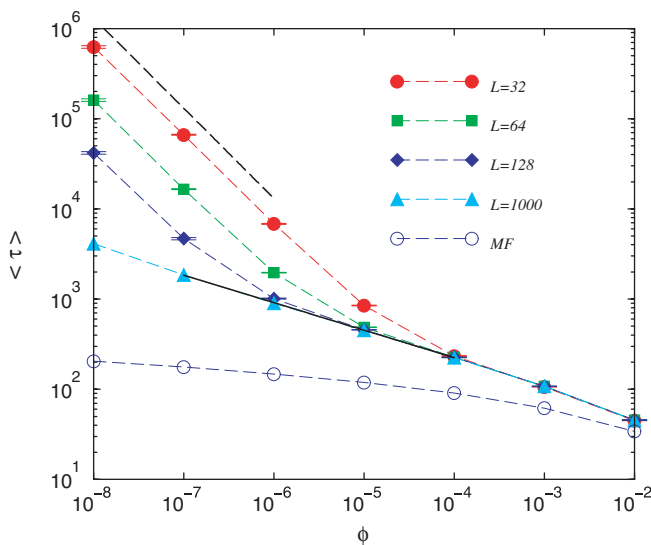


Fig. 10. Average lifetime (in units of MCSS) vs. the mutation rate on log-log scales for  $\alpha_1 = 0.50$ ,  $\alpha_2 = 0.70$ , and  $\mu = 0.20$  for various system sizes  $L$ . The straight solid line (fitted across data points for  $L = 1000$ ) is the best-fit power function indicating the  $\langle \tau \rangle \sim \phi^{-0.3}$  behavior [cf. Eq. (8)] in multi-cluster regime. The straight dashed line corresponds to a slope  $-1$ , indicating the  $\langle \tau \rangle \sim \phi^{-1}$  behavior in the single-cluster regime [cf. Eq. (7)]. For comparison, the lifetime in the mean-field (MF) approximation, obtained by solving Eq. (A.2) numerically, is also shown.

behavior of global densities in the spatially structured process (Duryea et al., 1999; Neuhauser and Pacala, 1999; Bolker et al., 2000). The time-dependent global densities of the respective alleles are

$$\rho_g(t) = (1/L^2) \sum_{\mathbf{x}} n_g(\mathbf{x}, t); \quad g = 1, 2. \quad (\text{A.1})$$

Given the local transition rates in Expression (2), the MF equations are

$$\begin{aligned} d\rho_1/dt &= \alpha_1\rho_1(1 - \rho_1 - \rho_2) - \mu\rho_1 + \phi(\rho_2 - \rho_1), \\ d\rho_2/dt &= \alpha_2\rho_2(1 - \rho_1 - \rho_2) - \mu\rho_2 + \phi(\rho_1 - \rho_2). \end{aligned} \quad (\text{A.2})$$

To highlight competition between the two alleles, we temporarily ignore mutation by setting  $\phi = 0$  ( $\phi$  is much smaller than other model parameters). Eqs. (A.2) exhibit three equilibrium (or stationary) points  $(\rho_1^*, \rho_2^*)$ . None permits coexistence; pre-emptive competition treats the genotypes as having completely overlapping niches (Amarasekare, 2003). For  $\alpha_1 < \mu$  and  $\alpha_2 < \mu$ , neither allele can persist dynamically, and the stable stationary point is  $(\rho_1^*, \rho_2^*) = (0, 0)$ ; the text refers to equilibrium mutual extinction as “phase 0.” Keeping  $\mu$  fixed, for  $\alpha_1 > \mu$  and  $\alpha_1 > \alpha_2$ , allele 1 competitively excludes allele 2 at equilibrium. In this case  $(\rho_1^*, \rho_2^*) = (1 - \mu/\alpha_1, 0)$  is stable, referred to as “phase 1.” If  $\alpha_2 > \mu$  and  $\alpha_1 < \alpha_2$ , allele 2 prevails by competitively excluding allele 1 and  $(\rho_1^*, \rho_2^*) = (0, 1 - \mu/\alpha_2)$  is stable, referred to as “phase 2.” The transition between phase 1 and mutual extinction (phase 0) is continuous in that the density of allele 1 vanishes continuously as  $\alpha_1 \rightarrow \alpha_c$  from above, where the critical rate is  $\alpha_c = \mu$ . In particular, in the vicinity of the critical point, the equilibrium density of allele 1 increases linearly with  $\alpha_1$ ,  $\rho_1^* \approx (\alpha_1 - \alpha_c)/\mu$ . The transition between phases 2 and 0, invader extinction, is identical by symmetry. In the presence of rare mutations, our MF model predicts that when  $\phi \ll \mu < \alpha_1 < \alpha_2$ , the resident allele (allele 1), resting at its positive equilibrium density, will be invaded by the alternate allele (allele 2). The invader will then advance to exclude the resident competitively (to density of order  $\phi$ ).

In the absence of mutation ( $\phi = 0$ ), the transition between the two positive equilibria, phases 1 and 2, is discontinuous. The densities exhibit a “jump” of size  $1 - \mu/\alpha$  crossing the line of competitive equivalence, where clonal propagation rates of the two alleles are equal:  $\alpha_1 = \alpha_2 = \alpha$ . Given rare mutation ( $0 < \phi \ll 1$ ), this transition becomes a very narrow crossover (with a width of order  $\phi$ ) through which the densities change sharply, but continuously, between phases 1 and 2. Away from this crossover region (so that  $|\alpha_2 - \alpha_1| \gg \phi$ ), the densities are well approximated by those of the case where  $\phi = 0$ , with small corrections (of order  $\phi$ ).

### A.2. Pair approximation

Pair approximation (PA) (Dickman, 1986; Matsuda et al., 1987; Bauch and Rand, 2000; Satō and Iwasa, 2000;

van Baalen, 2000) incorporates correlations of nearest neighbors into the dynamics, and consequently may predict equilibrium densities more accurately than MF models (Ellner et al., 1998; Caraco et al., 2001; Tainaka, 2003). Appendix B presents details of our model's PA. In the invader's absence (with  $\phi = 0$ ), PA predicts an equilibrium global density for the resident allele that depends on neighborhood size,  $\rho_1^* = [\delta - 1 - \delta(\mu/\alpha_1)]/[\delta - 1 - (\mu/\alpha_1)]$ ; simulations indicate improvement over the MF prediction. Compared to the MF result, PA (for fixed  $\mu$ ) increases the critical value of the propagation rate  $\alpha_c$  in the continuous phase transition between extinction and persistence. Under PA  $\alpha_c = \mu\delta/(\delta - 1)$ , so that  $\alpha_c$  decreases as neighborhood size increases. Spatially clustered growth increases the probability that a site neighboring an individual is occupied beyond the occupation probability of a randomly chosen site. Consequently, persistence under PA requires a greater propagation rate than is required under homogeneous mixing, since propagules are wasted on occupied neighboring sites. Nevertheless, PA preserves the MF model's linear behavior in the vicinity of the critical point,  $\rho_1^* \approx (\alpha_1 - \alpha_c)/\mu$ . The transition between phases 2 and 0, invader extinction, is, again, identical by symmetry. Further, the transition (crossover) between phases 1 and 2 occurs at  $\alpha_1 = \alpha_2$ .

### A.3. Monte Carlo phase diagram for equilibrium

To explore the spatially detailed model's equilibrium behavior, we carried out Monte Carlo (MC) simulations on  $L \times L$  square lattices with periodic boundaries. The model's equilibrium phase diagram, Fig. 1(a), agrees qualitatively with the results of the MF and PA discussed above. The two positive equilibria (where one allele excludes its competitor), phases 1 and 2, exhibit a transition (through a very narrow, continuous crossover) across the line  $\alpha_1 = \alpha_2$ , reflecting symmetry of the local dynamics; see Fig. 1(b). The fully spatial system also exhibits mutual extinction (phase 0) for  $\alpha_1 < \alpha_c$  and  $\alpha_2 < \alpha_c$ , where  $\alpha_c$  depends on  $\mu$ . The transition between positive density and extinction (alleles cannot advance when  $\alpha_g < \alpha_c$ ,  $g = 1, 2$ ) is continuous. The behavior of the resident's equilibrium global density (phase 1) near the critical point,  $\alpha_c \approx 1.65\mu$ , is described by a non-trivial power-law,  $\rho_1^* \propto (\alpha_1 - \alpha_c)^\beta$  with  $\beta \approx 0.58$ ; see Fig 1(c). Hence neither the MF nor PA model captures quantitative detail of the continuous transition near extinction; both underestimate the propagation rate where extinction occurs, and more importantly, fail to predict the correct power-law near the transition. The transition between phase 2, where allele 2 rests at positive equilibrium, and extinction is identical by symmetry.

This continuous transition occurs between (what we may term) an active state, positive equilibrium density, and a single absorbing state, extinction. Therefore, it is expected to fall into the directed percolation (DP) universality class (reviewed by Hinrichsen, 2000), a technical point that leads

to an ecological generality. The lattice model involves three distinct, elementary states: resident, invader, and empty sites (holes). But consider the dynamics for  $\alpha_2 < \alpha_c$  as  $\alpha_1$  is varied, where the continuous phase transition between the resident allele's persistence and extinction occurs. Since the mutation rate is small, allele 2 plays essentially no role in the dynamics. The model effectively translates to a one-allele (particles and holes) system governed by the local propagation and mortality rates of that single allele. [Oborny et al. \(2005\)](#) have shown that this sort of one-type spatial model is equivalent to the contact process ([Harris, 1974](#); [Levin and Pacala, 1997](#)). The latter has been investigated thoroughly using MC and renormalization-group methods of statistical physics, and been shown to belong to the DP universality class ([Grassberger and de la Torre, 1979](#); [Marro and Dickman, 1999](#); [Hinrichsen, 2000](#)), where spatial correlations between population density fluctuations can span the full system as the critical point is approached ([Stanley, 1971](#)). Consequently, MF, PA, and similar approximations based on truncating correlations, will break down ([Petermann and De Los Rios, 2004](#)). Values we found for the critical propagation rate ( $\alpha_c \approx 1.65\mu$ ) and the power-law exponent of the density of the extant allele near extinction ( $\beta \approx 0.58$ ) agree very well with those of the two-dimensional contact process ([Hinrichsen, 2000](#)), as [Oborny et al. \(2005\)](#) observed in their single-species model. We further verified that fluctuations of the global density rapidly increase (also in a power-law fashion) as the critical point is approached, indicating that this transition is “critical.” These fluctuations imply the possibility of stochastic extinction even above the critical colonization rate for any finite system, a property underlying the ecological significance of dispersal-limited extinction ([Oborny et al., 2005](#)).

## Appendix B. Pair approximation

Pair approximation tracks the deterministic dynamics of both global densities and local densities conditioned on the state of a neighboring site ([Rand, 1999](#)). The text defines global densities  $\rho_g$ . For local densities, suppose that site  $\mathbf{x}$  has elementary state  $j$ .  $q_{k/j}$  is the conditional probability that a randomly selected site on the neighborhood of site  $\mathbf{x}$  has state  $k$ . By conditional probability:

$$q_{0/j} + q_{1/j} + q_{2/j} = 1 \quad (j = 0, 1, 2), \quad (\text{B.1})$$

where  $j$  indicates empty (0), resident-occupied (1) and invader-occupied (2) sites; see Expression (2) in the text. The dynamics of local densities involves global pair densities  $\rho_{jk}$ , the unconditional probability that site  $\mathbf{x}$  has elementary state  $j$ , and a randomly chosen nearest neighbor of site  $\mathbf{x}$  has state  $k$ . We assume spatial symmetry,  $\rho_{jk} = \rho_{kj}$ , so that:

$$q_{k/j} = (\rho_k/\rho_j)q_{j/k}. \quad (\text{B.2})$$

Equality constraints and spatial symmetry imply that five equations specify the PA; we write equations for  $\rho_1$ ,  $\rho_2$ ,  $q_{1/1}$ ,  $q_{1/2}$ , and  $q_{2/2}$ . We can define the remaining seven variables in terms of the five variables the dynamics tracks. To do so, we follow [Iwasa et al. \(1998\)](#).

Under PA the invader allele's global density evolves according to:

$$d\rho_2/dt = \alpha_2 q_{0/2} \rho_2 + \phi(\rho_1 - \rho_2) - \mu \rho_2. \quad (\text{B.3})$$

The respective terms represent local growth, mutation, and mortality.  $q_{0/2}$  is the fraction of the sites neighboring a site occupied by the invader that, on average, is empty.

Rewritten in terms of the five dynamic variables, Eq. (B.3) becomes:

$$d\rho_2/dt = \alpha_2 \rho_2 (1 - q_{1/2} - q_{2/2}) + \phi(\rho_1 - \rho_2) - \mu \rho_2. \quad (\text{B.4})$$

To write the dynamics of a local density, we require the dynamics of the corresponding doublet, a global density. First, consider the global-pair density  $\rho_{22}$ , the frequency of invader-allele pairs among all neighboring-site pairs.  $\rho_{22}$  has dynamics:

$$d\rho_{22}/dt = 2\phi(\rho_{12} - \rho_{22}) - 2\mu\rho_{22} + 2\rho_{02} \left[ \frac{\alpha_2}{\delta} + (\delta - 1) \frac{\alpha_2}{\delta} q_{2/02} \right]. \quad (\text{B.5})$$

The first two terms represent net mutation and mortality, respectively. The third represents local propagation into the empty site of empty-invader and invader-empty pairs. An invader occupies one site in each such pair, colonizing the empty site at rate  $\alpha_2/\delta$ . Each of the remaining neighbors of the empty site may, or may not, be occupied by an invader. The conditional probability that an invader allele occupies a third site neighboring the open site of an empty-invader pair is  $q_{2/02}$ . Ordinary PA assumes that  $q_{2/02} \approx q_{2/0}$ , and replaces the former with the latter, allowing closure of the system of equations ([van Baalen, 2000](#)). Replacing  $q_{2/02}$  with  $q_{2/0}$  in Eq. (B.5), rewriting in terms of the state variables and rearranging yields:

$$d\rho_{22}/dt = 2\rho_2 [\phi(q_{1/2} - q_{2/2}) - \mu q_{2/2}] + 2\rho_2 (1 - q_{1/2} - q_{2/2}) \times \left[ \frac{\alpha_2}{\delta} \left( 1 + [\delta - 1] \frac{\rho_2}{1 - \rho_1 - \rho_2} \times [1 - q_{1/2} - q_{2/2}] \right) \right]. \quad (\text{B.6})$$

Since  $q_{i/i} = \rho_{ii}/\rho_i$ , we note ([Satō and Iwasa, 2000](#)):

$$dq_{2/2}/dt = (1/\rho_2)(d\rho_{22}/dt) - (1/\rho_2)q_{2/2}(d\rho_2/dt).$$

Then, using Eqs. (B.5) and (B.6), we have the conditional-density dynamics  $dq_{2/2}/dt$ :

$$dq_{2/2}/dt = 2(1 - q_{1/2} - q_{2/2}) \times \left[ \frac{\alpha_2}{\delta} \left( 1 + [\delta - 1] \frac{\rho_2}{1 - \rho_1 - \rho_2} \right) \times [1 - q_{1/2} - q_{2/2}] \right] + 2\phi(q_{1/2} - q_{2/2}) - q_{2/2} \times \left[ \alpha_2(1 - q_{1/2} - q_{2/2}) + \frac{\phi(\rho_1 - \rho_2)}{\rho_2} + \mu \right]. \quad (\text{B.7})$$

The resident's global density evolves according to

$$d\rho_1/dt = \alpha_1 q_{0/1} \rho_1 + \phi(\rho_2 - \rho_1) - \mu \rho_1. \quad (\text{B.8})$$

The terms refer to local propagation, net effect of mutation, and mortality. Rewriting in terms of the five dynamic variables yields:

$$d\rho_1/dt = \alpha_1 \rho_1 \left( 1 - q_{1/1} - \left( \frac{\rho_2}{\rho_1} \right) q_{1/2} \right) + \phi(\rho_2 - \rho_1) - \mu \rho_1. \quad (\text{B.9})$$

To obtain  $dq_{1/2}/dt$ , we begin with the doublet  $\rho_{12}$ :

$$d\rho_{12}/dt = \phi(\rho_1 q_{1/1} + \rho_2 q_{2/2}) - 2\mu \rho_2 q_{1/2} + \frac{\delta - 1}{\delta} \frac{\rho_1 \rho_2}{1 - \rho_1 - \rho_2} \left[ 1 - \frac{\rho_2}{\rho_1} q_{1/2} - q_{1/1} \right] \times (1 - q_{1/2} - q_{2/2})(\alpha_2 + \alpha_1). \quad (\text{B.10})$$

Since  $q_{1/2} = \rho_{12}/\rho_2$ ,

$$dq_{1/2}/dt = (1/\rho_2)(d\rho_{12}/dt) - (1/\rho_2)q_{1/2}(d\rho_2/dt).$$

Using Eqs. (B.4) and (B.10), we have the conditional-density dynamics:

$$dq_{1/2}/dt = \phi \left( \frac{\rho_1}{\rho_2} q_{1/1} + q_{2/2} \right) - q_{1/2} \mu + \frac{\delta - 1}{\delta} \frac{\rho_1}{1 - \rho_1 - \rho_2} \left[ 1 - \frac{\rho_2}{\rho_1} q_{1/2} - q_{1/1} \right] \times (1 - q_{1/2} - q_{2/2})(\alpha_2 + \alpha_1) - q_{1/2} \left[ \alpha_2(1 - q_{1/2} - q_{2/2}) + \frac{\phi(\rho_1 - \rho_2)}{\rho_2} \right]. \quad (\text{B.11})$$

To obtain  $dq_{1/1}/dt$ , we begin with the doublet  $\rho_{11}$ :

$$d\rho_{11}/dt = 2\phi(\rho_2 q_{1/2} - \rho_1 q_{1/1}) - 2\mu \rho_1 q_{1/1} + 2\rho_1 \left[ 1 - \frac{\rho_2}{\rho_1} q_{1/2} - q_{1/1} \right] \times \left[ \frac{\alpha_1}{\delta} \left( 1 + [\delta - 1] \left[ \frac{\rho_1}{1 - \rho_1 - \rho_2} \right] \right) \times \left( 1 - \frac{\rho_2}{\rho_1} q_{1/2} - q_{1/1} \right) \right]. \quad (\text{B.12})$$

We recognize that:

$$dq_{1/1}/dt = (1/\rho_1)(d\rho_{11}/dt) - (1/\rho_1)q_{1/1}(d\rho_1/dt).$$

This leads to the conditional-density dynamics:

$$dq_{1/1}/dt = 2 \left[ 1 - \frac{\rho_2}{\rho_1} q_{1/2} - q_{1/1} \right] \times \left[ \frac{\alpha_1}{\delta} \left( 1 + [\delta - 1] \left[ \frac{\rho_1}{1 - \rho_1 - \rho_2} \right] \right) \times \left( 1 - \frac{\rho_2}{\rho_1} q_{1/2} - q_{1/1} \right) \right] + 2\phi \left( \frac{\rho_2}{\rho_1} q_{1/2} - q_{1/1} \right) - q_{1/1} \times \left[ \alpha_1 \left( 1 - q_{1/1} - \frac{\rho_2}{\rho_1} q_{1/2} \right) + \frac{\phi(\rho_2 - \rho_1)}{\rho_1} + \mu \right]. \quad (\text{B.13})$$

This equation completes the PA system.

### B.1. Resident at equilibrium

If  $\phi = \rho_2 = 0$  in Eq. (B.9) we find

$$q_{1/1}^* = 1 - \frac{\mu}{\alpha_1}. \quad (\text{B.14})$$

Using this result in Eq. (B.13), with  $\phi = 0$  and  $\rho_2 = 0$ , yields the resident's equilibrium global density, in the absence of the advantageous allele, under PA:

$$\rho_1^* = \frac{\delta - 1 - \delta(\mu/\alpha_1)}{\delta - 1 - (\mu/\alpha_1)}, \quad (\text{B.15})$$

which is smaller than the MF equilibrium density,  $\rho_1^* = 1 - \mu/\alpha_1$ .

### B.2. Deterministic condition for initial spread of the advantageous allele

Now we assume that mutation already has introduced the invader allele, and we set the mutation rate  $\phi = 0$  in both genotypes. The analysis then approximates the expected outcome for an initial cluster of the invader allele (van Baalen, 2000).

Any increase in the invader allele's density requires  $d\rho_2/dt > 0$ . Evaluated at  $\phi = 0$ , this condition implies:

$$1 - q_{1/2} - q_{2/2} > \left( \frac{\mu}{\alpha_2} \right). \quad (\text{B.16})$$

That is, given that an invader occupies an arbitrary site, the conditional density of empty sites on the invader's neighborhood must exceed the invader's mortality to propagation-rate ratio for the advantageous allele to advance when rare. We evaluate the conditional densities in Expression (B.16) to predict the invader allele's advance when rare.

Proceeding as in Iwasa et al. (1998), we solve the dynamics in the local environment of a rare invader allele, using the resident-only equilibria,  $\rho_1^*$  and  $q_{1/1}^*$  with  $\rho_2 = 0$ . That is, given the results in (B.14) and (B.15), we find equilibrium values for  $q_{1/2}$  and  $q_{2/2}$  when the invader is rare. Finally, we use these equilibria to evaluate Expression (B.16), the condition for positive growth of the invader's global density. Although the invader is globally rare, local clustering implies that  $q_{2/2}$  need not be close to zero.

Using Eqs. (B.14) and (B.15) in Eqs. (B.7) and (B.11) yields:

$$q_{1/2} = \frac{\left(\delta - 1 - \frac{\delta\mu}{\alpha_1}\right)(1 - q_{1/2} - q_{2/2})\left(\frac{\alpha_2 + \alpha_1}{\delta}\right)}{\alpha_2(1 - q_{1/2} - q_{2/2}) + \mu}, \quad (\text{B.17})$$

and

$$q_{2/2} = \frac{2(1 - q_{1/2} - q_{2/2})\left(\frac{\alpha_2}{\delta}\right)}{\alpha_2(1 - q_{1/2} - q_{2/2}) + \mu}, \quad (\text{B.18})$$

where (B.17) and (B.18) assume dynamic equilibrium.

$(1 - q_{1/2} - q_{2/2})$  is the conditional density of empty sites, given that a rare invader occupies the focal site. We know that the quantity  $q_{0/2} = (1 - q_{1/2} - q_{2/2})$  must exceed  $\mu/\alpha_2$  for the invader allele to advance when rare, by Expression (B.16). Therefore, the sum  $(\mu/\alpha_2 + q_{1/2} + q_{2/2})$  must be less than 1, if the rare allele is to advance. Paralleling Iwasa et al. (1998), the condition for advance of the invader allele when rare, from Expression (B.16), is

$$\frac{\mu}{\alpha_2} + \frac{1}{\delta} + \frac{1}{2\alpha_2}(\alpha_2 + \alpha_1)\left(\frac{\delta - 1}{\delta} - \frac{\mu}{\alpha_1}\right) < 1. \quad (\text{B.19})$$

Expression (B.19) holds, and the rare allele invades, only if  $\alpha_2 > \alpha_1$ . By construction, PA yields the same deterministic criterion for invasion by the invader allele as obtained in the MF model. However, the predicted equilibrium densities differ between PA and MF models, and the difference depends on neighborhood size.

## References

- Amarasekare, P., 2003. Competitive coexistence in spatially structured environments: a synthesis. *Ecol. Lett.* 6, 1109–1122.
- Avrami, M., 1940. Kinetics of phase change. II. Transformation-time relations for random distribution of nuclei. *J. Chem. Phys.* 8, 212–240.
- Bauch, C., Rand, D.A., 2000. A moment closure model for sexually transmitted disease transmission through a concurrent partnership network. *Proc. R. Soc. London B* 267, 2019–2027.
- Ben-Naim, E., Krapivsky, P.L., 1996. Nucleation and growth in one dimension. *Phys. Rev. E* 54, 3562–3568.
- Bolker, B., Pacala, S.W., 1999. Spatial moment equations for plant competition: understanding spatial strategies and the advantage of short dispersal. *Am. Nat.* 153, 575–602.
- Bolker, B., Pacala, S.W., Levin, S.A., 2000. Moment equations for ecological processes in continuous space. In: Dieckmann, U., Law, R., Metz, J.A.J. (Eds.), *The Geometry of Ecological Interactions*. Cambridge University Press, Cambridge, pp. 399–411.
- Cantrell, R.S., Cosner, C., 1991. The effect of spatial heterogeneity in population dynamics. *J. Math. Biol.* 29, 315–338.
- Caraco, T., Duryea, M.C., Glavanakov, S., Maniatty, W., Szymanski, B.K., 2001. Host spatial heterogeneity and the spread of vector-borne infection. *Theor. Popul. Biol.* 59, 185–206.
- Caraco, T., Glavanakov, S., Chen, G., Flaherty, J.E., Ohsumi, T.K., Szymanski, B.K., 2002. Stage-structured infection transmission and a spatial epidemic: a model for Lyme disease. *Am. Nat.* 160, 348–359.
- Caraco, T., Glavanakov, S., Li, S., Maniatty, W., Szymanski, B.K., 2006. Spatially structured superinfection and the evolution of disease virulence. *Theor. Popul. Biol.* 69, 367–384.
- Chesson, P., 2000. General theory of competitive coexistence in spatially-varying environments. *Theor. Popul. Biol.* 58, 211–237.
- Chesson, P., Lee, C.T., 2005. Families of discrete kernels for modeling dispersal. *Theor. Popul. Biol.* 67, 241–256.
- Claessen, D., de Roos, A.M., 1995. Evolution of virulence in a host-pathogen system with local pathogen transmission. *Oikos* 74, 401–413.
- Dickman, R., 1986. Kinetic phase transitions in a surface-reaction model: mean-field theory. *Phys. Rev. A* 34, 4246–4250.
- Duiker, H.M., Beale, P.D., 1990. Grain-size effects in ferroelectric switching. *Phys. Rev. B* 41, 490–495.
- Durrett, R., Levin, S.A., 1994a. The importance of being discrete (and spatial). *Theor. Popul. Biol.* 46, 363–394.
- Durrett, R., Levin, S.A., 1994b. Stochastic spatial models: a user's guide to ecological applications. *Philos. Trans. R. Soc. London B* 343, 329–350.
- Durrett, R., Levin, S.A., 1998. Spatial aspects of interspecific competition. *Theor. Popul. Biol.* 53, 30–43.
- Duryea, M., Caraco, T., Gardner, G., Maniatty, W., Szymanski, B.K., 1999. Population dispersion and equilibrium infection frequency in a spatial epidemic. *Physica D* 132, 511–519.
- Ellner, S.P., Sasaki, A., Haraguchi, Y., Matsuda, H., 1998. Speed of invasion in lattice population models: pair-edge approximation. *J. Math. Biol.* 36, 469–484.
- Fife, P.C., 1979. *Mathematical Aspects of Reacting and Diffusing Systems*. Springer, Berlin.
- Fisher, R.A., 1937. The wave of advance of advantageous genes. *Ann. Eugen. London* 7, 355–369.
- Frantzen, J., van den Bosch, F., 2000. Spread of organisms: can travelling and dispersive waves be distinguished? *Basic Appl. Ecol.* 1, 83–91.
- Gandhi, A., Levin, S., Orszag, S., 1999. Nucleation and relaxation from meta-stability in spatial ecological models. *J. Theor. Biol.* 200, 121–146.
- Grassberger, P., de la Torre, A., 1979. Reggeon field theory (Schlögl's second model) on a lattice: Monte Carlo calculations of critical behavior. *Ann. Phys.* 122, 373–396.
- Harris, T.E., 1974. Contact interaction on a lattice. *Ann. Probab.* 2, 969–988.
- Herrick, J., Jun, S., Bechhoefer, J., Bensimon, A., 2002. Kinetic model of DNA replication in eukaryotic organisms. *J. Mol. Biol.* 320, 741–750.
- Hinrichsen, H., 2000. Non-equilibrium critical phenomena and phase transitions into absorbing states. *Adv. Phys.* 49, 815–958.
- Holmes, E.E., Lewis, M.A., Banks, J.E., Veit, R.R., 1994. Partial differential equations in ecology: spatial interactions and population dynamics. *Ecology* 75, 17–29.
- Ishibashi, Y., Takagi, Y., 1971. Note on ferroelectric domain switching. *J. Phys. Soc. Japan* 31, 506–510.
- Iwasa, Y., Nakamura, M., Levin, S.A., 1998. Allelopathy of bacteria in a lattice population: competition between colicin-sensitive and colicin-producing strains. *Evol. Ecology* 12, 785–802.
- Johnson, W.A., Mehl, R.F., 1939. Reaction kinetics in processes of nucleation and growth. *Trans. Am. Inst. Min. Metall. Eng.* 135, 416–442.
- Karttunen, M., Provatas, N., Ala-Nissila, T., Grant, M., 1998. Nucleation, growth, and scaling in slow combustion. *J. Stat. Phys.* 90, 1401–1411.
- Kolmogorov, A.N., 1937. A statistical theory for the recrystallization of metals. *Bull. Acad. Sci. USSR, Phys. Ser.* 1, 355–359.
- Kolmogorov, A., Petrovsky, N., Piskounov, N.S., 1937. A study of the equation of diffusion with increase in the quantity of matter, and its

- application to a biological problem. *Moscow Univ. Bull. Math.* 1, 1–25.
- Korniss, G., Caraco, T., 2005. Spatial dynamics of invasion: the geometry of introduced species. *J. Theor. Biol.* 233, 137–150.
- Korniss, G., Novotny, M.A., Rikvold, P.A., 1999. Parallelization of a dynamic Monte Carlo algorithm: a partially rejection-free conservative approach. *J. Comput. Phys.* 153, 488–494.
- Kot, M., Lewis, M.A., van den Driessche, P., 1996. Dispersal data and the spread of invading organisms. *Ecology* 77, 2027–2042.
- Levin, S.A., Pacala, S.W., 1997. Theories of simplification and scaling in spatially distributed processes. In: Tilman, D., Kareiva, P. (Eds.), *Spatial Ecology: The Role of Space in Population Dynamics and Interspecific Interactions*. Princeton University Press, Princeton, pp. 271–295.
- Levin, S.A., Grenfell, B., Hastings, A., Perelson, A.S., 1997. Mathematical and computational challenges in population biology and ecosystems science. *Science* 275, 334–343.
- Lewis, M.A., Kareiva, P., 1993. Allee dynamics and the spread of invading organisms. *Theor. Popul. Biol.* 43, 141–158.
- Lewis, M.A., Pacala, S.W., 2000. Modeling and analysis of stochastic invasion processes. *J. Math. Biol.* 41, 387–429.
- Machado, E., Buendía, G.M., Rikvold, P.A., 2005. Decay of metastable phases in a model for the catalytic oxidation of CO. *Phys. Rev. E* 71, 031603, (12pp).
- Marro, J., Dickman, R., 1999. *Nonequilibrium Phase Transitions in Lattice Models*. Cambridge University Press, Cambridge, UK.
- Matsuda, H., Tamachi, N., Ogita, A., Sasaki, A., 1987. A lattice model for population biology. In: Teramoto, E., Yamaguti, M. (Eds.), *Mathematical Topics in Biology: Lecture Notes in Biomathematics*, vol. 71. Springer, New York, pp. 154–161.
- Metz, J.A.J., Mollison, D., van den Bosch, F., 2000. The dynamics of invasion waves. In: Dieckmann, U., Law, R., Metz, J.A.J. (Eds.), *The Geometry of Ecological Interactions*. Cambridge University Press, Cambridge, pp. 482–512.
- Murray, J.D., 2003. *Mathematical Biology*, vol. II. Springer, New York.
- Neubert, M.G., Caswell, H., 2000. Demography and dispersal: calculation and sensitivity analysis of invasion speed for structured populations. *Ecology* 81, 1613–1628.
- Neubert, M.G., Kot, M., Lewis, M.A., 1995. Dispersal and pattern formation in a discrete-time predator-prey model. *Theor. Popul. Biol.* 48, 7–43.
- Neuhauser, C., Pacala, S.W., 1999. An explicitly spatial version of the Lotka–Volterra model with interspecific competition. *Ann. Appl. Probab.* 9, 1226–1259.
- Oborny, B., Meszéna, G., Szabó, G., 2005. Dynamics of populations on the verge of extinction. *Oikos* 109, 291–296.
- Okubo, A., 1980. *Diffusion and Ecological Problems: Mathematical Models*. Springer, Berlin.
- O'Malley, L., Allstadt, A., Korniss, G., Caraco, T., 2005. Nucleation and global time scales in ecological invasion under pre-emptive competition. In: Stocks, N.G., Abbott, D., Morse, R.P. (Eds.), *Fluctuations and Noise in Biological, Biophysical, and Biomedical Systems*, vol. III. Proceedings of SPIE, vol. 5841. SPIE, Bellingham WA, pp. 117–124.
- O'Malley, L., Kozma, B., Korniss, G., Rácz, Z., Caraco, T., in press. Fisher waves and the velocity of front propagation in a two-species invasion model with preemptive competition. In: Landau, D.P., Lewis, S.P., Schüttler, H.-B. (Eds.), *Computer Simulation Studies in Condensed Matter Physics*, vol. XIX. Springer Proceedings in Physics. Springer, Heidelberg, Berlin <<http://arxiv.org/abs/q-bio.PE/0603013>>.
- Petermann, T., De Los Rios, P., 2004. Cluster approximations for epidemic processes: a systematic description of correlations beyond the pair level. *J. Theor. Biol.* 229, 1–11.
- Ramos, R.A., Rikvold, P.A., Novotny, M.A., 1999. Test of the Kolmogorov–Johnson–Mehl–Avrami picture of meta-stable decay in a model with microscopic dynamics. *Phys. Rev. B* 59, 9053–9069.
- Rand, D.A., 1999. Correlation equations and pair approximations for spatial ecologies. In: McGlade, J.M. (Ed.), *Advanced Ecological Theory: Principles and Applications*. Blackwell, Oxford, pp. 100–142.
- Richards, H.L., Sides, S.W., Novotny, M.A., Rikvold, P.A., 1995. Magnetization switching in nanoscale ferromagnetic grains: description by a kinetic Ising model. *J. Magn. Mater.* 150, 37–50.
- Rikvold, P.A., Tomita, H., Miyashita, S., Sides, S.W., 1994. Metastable lifetimes in a kinetic Ising model: dependence on field and system size. *Phys. Rev. E* 49, 5080–5090.
- Satō, K., Iwasa, Y., 2000. Pair approximations for lattice-based ecological models. In: Dieckmann, U., Law, R., Metz, J.A.J. (Eds.), *The Geometry of Ecological Interactions*. Cambridge University Press, Cambridge, pp. 341–358.
- Seabloom, E.W., Bjornstad, O.N., Bolker, B.M., Reichman, O.J., 2005. Spatial signature of environmental heterogeneity, dispersal, and competition in successional grasslands. *Ecology* 75, 199–214.
- Shurin, J.B., Amarasekare, P., Chase, J.M., Holt, R.D., Hoopes, M.F., Leibold, M.A., 2004. Alternative stable states and regional community structure. *J. Theor. Biol.* 227, 359–368.
- Stanley, H.E., 1971. *Introduction to Phase Transitions and Critical Phenomena*. Clarendon Press, New York.
- Tainaka, K., 2003. Lattice model for the Lotka–Volterra system. *J. Phys. Soc. Japan* 57, 2588–2590.
- Tainaka, K., Kushida, M., Itoh, Y., Yoshimura, J., 2004. Interspecific segregation in a lattice ecosystem with intraspecific competition. *J. Phys. Soc. Japan* 73, 2914–2915.
- Thomson, N.A., Ellner, S.P., 2003. Pair-edge approximation for heterogeneous lattice models. *Theor. Popul. Biol.* 64, 271–280.
- van Baalen, M., 2000. Pair approximations for different spatial geometries. In: Dieckmann, U., Law, R., Metz, J.A.J. (Eds.), *The Geometry of Ecological Interactions*. Cambridge University Press, Cambridge, pp. 359–387.
- van Baalen, M., Rand, D.A., 1998. The unit of selection in viscous populations and the evolution of altruism. *J. Theor. Biol.* 193, 631–648.
- van den Bosch, F., Metz, J.A.J., Dieckmann, O., 1990. The velocity of spatial population expansion. *J. Math. Biol.* 28, 529–565.
- van den Bosch, F., Hengeveld, R., Metz, J.A.J., 1992. Analysing the velocity of animal range expansion. *J. Biogeo.* 19, 135–150.
- Wei, W., Krone, S.M., 2005. Spatial invasion by a mutant pathogen. *J. Theor. Biol.* 236, 335–348.
- Wilson, W.G., 1998. Resolving discrepancies between deterministic population models and individual-based simulations. *Am. Nat.* 151, 116–134.
- Wilson, W.G., de Roos, A.M., McCauley, E., 1993. Spatial instabilities within the diffusive Lotka–Volterra system: individual-based simulation results. *Theor. Popul. Biol.* 43, 91–127.
- Yasi, J.A., Korniss, G., Caraco, T., in press. Invasive allele spread under preemptive competition. In: Landau, D.P., Lewis, S.P., Schüttler, H.-B. (Eds.), *Computer Simulation Studies in Condensed Matter Physics*, vol. XVIII. Springer Proceedings in Physics. Springer, Heidelberg, Berlin <<http://arxiv.org/abs/cond-mat/0505523>>.
- Zadoks, J.-C., 2000. Foci, small and large: a specific class of biological invasion. In: Dieckmann, U., Law, R., Metz, J.A.J. (Eds.), *The Geometry of Ecological Interactions*. Cambridge University Press, Cambridge, pp. 292–317.